REPORT DOCUMENTATION PAGE

Form Approved
OMB NO. 0704-0188

1. AGENCY USE ONLY (Leave blank)	2. REPORT DATE	3. REPORT TYPE AND DATES COVERED
	1/29/99	FINAL

4. TITLE AND SUBTITLE
A Numerical and Experimental Study of Arcjet Fluctuation

5. FUNDING NUMBERS
F49620-94-1-0399

6. AUTHOR(S)
K. Powell, A. Gallimore, B. Van Leer

7. PERFORMING ORGANIZATION NAME(S) AND ADDRESS(ES)
Department of Aerospace Engineering
University of Michigan
Ann Arbor, MI 48109-2140

8. PERFORMING ORGANIZATION REPORT NUMBER
032333 FINAL

9. SPONSORING / MONITORING AGENCY NAMES(S) AND ADDRESS(ES)
AFOSR/NM
801 North Randolph Street, Room 732
Arlington, Virginia 22203-1977

10. SPONSORING / MONITORING AGENCY REPORT NUMBER

11. SUPLEMENTARY NOTES
The views, opinions and/or findings contained in this report are those of the author(s) and should not be construed as an official Department of the Army position, policy or decision, unless so designated by other documentation.

12a. DISTRIBUTION / AVAILABILITY STATEMENT

Approved for public release; distribution unlimited.

12b. DISTRIBUTION CODE

13. ABSTRACT (Maximum 200 words)
The work described here is a combined numerical/experiental study of arcjets. The focus of the experimental work has been a parametric study of the onset of instability in arc thruster devices. The focus of the numerical work has been the development of numerical methods for solving the magnetohydrodynamics (MHD) equations in complex geometries

14. SUBJECT TERMS

15. NUMBER IF PAGES

16. PRICE CODE

17. SECURITY CLASSIFICATION OR REPORT	18. SECURITY CLASSIFICATION OF THIS PAGE	19. SECURITY CLASSIFICATION OF ABSTRACT	20. LIMITATION OF ABSTRACT
UNCLASSIFIED	**UNCLASSIFIED**	**UNCLASSIFIED**	**UL**

A Numerical and Experimental Study of Arcjet Fluctuation
AFOSR Grant F49620-94-1-0399
Final Report

Ken Powell, Alec Gallimore and Bram van Leer
Department of Aerospace Engineering
University of Michigan
Ann Arbor, MI 48109-2140

January, 1999

Introduction

Electric arc heaters produce high-temperature gas which can be used for a number of purposes, including the generation of thrust for spacecraft propulsion, the synthesis of diamond and boron nitride films for industrial tool hardening and electrical insulation, respectively, and the generation of high-enthalpy, hypersonic air streams for the investigation of processes associated with ultra-high velocity atmospheric flight. As ubiquitous as electrical arcs are, understanding of them is limited. As such, attempts at extending the operating envelope of electrical arc devices (e.g. by increasing pressure) through empiricism alone can lead to unexpected and sometimes disastrous results.

The work described here is a combined numerical/experimental study of arcjets. The focus of the experimenal work has been a parametric study of the onset of instability in arc thruster devices. The focus of the numerical work has been the development of numerical methods for solving the magnetohydrodynamics (MHD) equations in complex geometries.

Summary of Experimental Work

High-enthalpy arc-tunnels enter an unstable operating regime when the working fluid mass flow rate is maintained at an incompatible value. A similar phenomenon is manifested in arc-producing propulsion systems (e.g., arcjets) in a process known as starvation, whereby the propellant flow rate is too low to adequately satisfy particle flux requirements of a stable arc. In order to determine how this phenomenon and others seen in arcjets may be used to understand arc-tunnel instabilities, the discharge current and voltage of a 1 kW arcjet were recorded as a function of mass flow rate by a digital oscilloscope. This was done to determine how propellant flow rate affects the stability of the arcjet discharge and to see how this information may be used in the development of a computer model. These measurements were performed with hydrogen as the propellant. In addition, near-field electron temperature and number density measurements were made via triple-Langmuir probe for comparison against code predictions. A 1 kW arcjet (Fig. 1) that was supplied by the NASA Lewis Research Center (LeRC) was used for this study. The arcjet was first developed as a by-product of arc [high-enthalpy] tunels used in the early space age to develop heat shields. An arcjet uses an arc to heat propellant (e.g., hydrogen) which is subsequently expanded through a nozzle. The arcjet used in this study features a 2%-thoriated tungsten cathode and a nozzle (also of 2%-thoriated tungsten) that serves as the anode. The arcjet has a 0.51-mm-diameter by 0.25-mm-long constrictor, a 30-degree half-angle converging nozzle section upstream of the constrictor, and a 20-degree half-angle diverging section. The exit diameter of the nozzle is 9.5 mm, giving the expansion section an area ratio of 350. The electrode gap spacing is 0.51 mm and the outer housing of the device is constructed of titaniated zirconiated molybdenum. The nominal exhaust velocity is approximately 8,000 m/s with hydrogen. All experiments reported were performed in the Plasmadynamics and Electric Propulsion Laboratory 6 m by 9 m vacuum chamber (Fig. 2). At the time of these tests, the chamber was pumped with six 81-cm-diamter oil diffusion pumps, two blowers and four mechanical pumps, providing a pumping speed of 300,000 l/s on hydrogen. Background chamber pressure was maintained to less than 1.5 x 10-4 Torr during arcjet operation. Since then, four CVI TM1200 reentrant cryopumps has been installed on the facility. Arcjet power was provided by a 1800 W Sorenson power supply that was conditioned by a NASA LeRC power processing unit (PPU). Arcjet

voltage was measured with Tektronix P6007 100:1 voltage probes clamped to the electrode leads on the vacuum chamber bulkhead. The voltage probe signals were collected by a Tektronix AM501 operational amplifier. Arcjet current is monitored with a Tektronix A6303 current sensor powered by a Tektronix AM503 current probe amplifier. Arcjet voltage and current data were monitored and recorded by a Tektronix TDS 540 digitizing oscilloscope, and stored on a computer via a GBIP interface and LabVIEW data acquisition system. The arcjet was operated at hydrogen flow rates of up to 10 SLM (15 mg/s). Propellant was supplied to the arcjet from compressed gas bottles through stainless-steel feed lines. Propellant flow was controlled and monitored with an MKS 1159B mass flow controller specially calibrated for light gases. A triple probe (Fig. 3) was used to measure ne and Te near the exit plane of the arcjet while running at 10 A, 79 V, and with a flow of 10 SLM. The probe was comprised of three individual tungsten wire electrodes, parallel to each other, 0.23 mm in diameter with an exposed length of 5.0 mm. Each wire was mounted in round single-bore alumina tubes which were held together with a high-temperature ceramic adhesive. The spacing between the electrodes was 1 mm. Two Duracell alkaline batteries were used to supply Vd3. Vd2, Vd3. These voltages as well as the current shunt voltage, Vsh, were directly fed to the LabVIEW data acquisition system. The probe was mounted on a large positioning system which contains two rotary platforms on a 6 ft-long radial stage that is mounted on a 3 ft travel axial stage. The probe was not rotated to be aligned with the flow due to time limitation. The errors due to probe misalignment with the flow will affect the radial measurements. This misalignment may result in artifically high Te and ne in some cases. The positioning system has an absolute position accuracy of 0.15 mm. Experimental Results Discharge Characteristics The discharge current and discharge voltage were recorded for each propellant flow rate using a digital oscilloscope. The data are shown in Figures 4 through 7. The horizontal scale (time scale) of the oscilloscope traces was chosen to be 20 s per division. This scale was selected to show clearly both the structures of the signals and the changes in those structures with varying flow rates at the same time. The oscillation of about 11 kHz in the discharge current and discharge voltage is caused by the oscillation in the output of the PPU. The discharge current remains constant at 10 A while the discharge voltage decreases as the flow rate decreases. This is due to the fact that the PPU is a constant-current power supply. The oscilloscope traces clearly indicate that

the structures in the discharge current and discharge voltage signals become "rattled" as the flow rate decreases and the arc becomes starved. It is not shown here that as the flow rate decreased, the repeatability of those signals suffered as well. The discharge current signals were less affected by the decrease of the flow rate than the discharge voltage signals. This is most likely due to the constant-current mode of the PPU. Although there is increased hash at the lower flow rates, the peak-to-peak values of the discharge current and discharge voltage signals do not vary significantly while the flow rate is changed. This may be due to the PPU as well. The oscilloscope traces also shows that there is a certain flow rateor a range around a certain flow rateat which the discharge switches to a "rattled mode." In this study, it was found to be at about 4.75 SLM of H2 flow. This result may be useful when one tries to save as much propellant as possible without destabilizing the discharge. This result may also be useful in the development of a computer code for arcjet operation. Plume Measurements Axial and radial profiles of the arcjet plume while the arcjet was running at 10 A/79 V with a H2 flow rate of 10 SLM were generated. Axial profile measurements of ne made with a triple probe along the axis of the arcjet from 5 mm to 300 mm downstream of the exit plane were presented in Fig. 8. These measurements show the electron temperature and number density to vary between 0.25 and 0.4 eV (2900-4600 K) and 1011 to 2 x 1012 cm-3, respectively. Radial profile measurements of ne and Te made with the same triple probe at 5 mm downstream of the exit plane were presented in Fig. 9. Figure 8 shows the comparison of centerline ne results from this study and a previous study.1 The two studies match well beyond 40 mm from the exit plane. Electron number densities measured in this study, however, is about half of those of the previous work for closer distances from the exit plane. The power level of the arcjet during the present experiments was 0.79 kW, which is about 20% less than the power level of 1 kW of Reference 1. Thus, the particle flux was less in this study than in the other study. This difference in particle flux due to lower engine power is small far from the exit plane because the flux of particles there is mostly due to diffusive processes. Fig. 9 shows the radial profile of ne and Te. It seems that there are two distinct regions separated at the radial position of 8 mm (more apparent in the Te profile). When the plume was observed visually, there were two distinct regions in the plume in a "co-annular cone." The inner cone was red, and the surrounding region was light blue. It should be noted that this two-color plume was not observed when the thruster ran at

1 kW of power. However, there might still have been the similar structure in the plume, though not readily visible. Conclusions The discharge current/voltage measurements at different flow rates suggest that the discharge becomes unstable as the propellant flow rate decreases, and that there exists a certain flow rate, or a small range around a certain flow rate, at which the discharge switches into a destabilized mode. The plume study suggests that there is a co-annular-cone-shaped structure in the arcjet plume. The study also indicates that 20 % reduction in the engine power results in 50 % decrease in the particle flux near the exit plane.

References

1. S. A. Bufton, R. L. Burton and H. Krier, "Measured Plasma Properties at the Exit Plane of a 1 kW Arcjet", AIAA-95-3066, 31st Joint Propulsion Conference, San Diego, CA, July 10-12, 1995

2. D. Tilley, A. Kelly and R. Jahn, "The Application of the Triple Probe Method to MPD Thruster Plumes", AIAA-90-2667, 21st International Electric Propulsion Conference, Orlando, FL, July 18-20, 1990

Summary of Numerical Work

The numerical modelling focused on solution of the ideal magnetohydrodynamic equations. The equations to be solved are those for conservation of mass, momentum, magnetic field and energy. They are solved in the form

$$\frac{\partial}{\partial t}\begin{pmatrix}\rho \\ \rho\mathbf{u} \\ \mathbf{B} \\ E\end{pmatrix} + \nabla\cdot\begin{pmatrix}\rho\mathbf{u} \\ \rho\mathbf{u}\mathbf{u}+\mathbf{I}\left(\mathbf{p}+\frac{\mathbf{B}\cdot\mathbf{B}}{2}\right)-\mathbf{B}\mathbf{B} \\ \mathbf{u}\mathbf{B}-\mathbf{B}\mathbf{u} \\ \left(E+p+\frac{\mathbf{B}\cdot\mathbf{B}}{2}\right)\mathbf{u}-\mathbf{B}\left(\mathbf{u}\cdot\mathbf{B}\right)\end{pmatrix} = -\begin{pmatrix}0 \\ \mathbf{B} \\ \mathbf{u} \\ \mathbf{u}\cdot\mathbf{B}\end{pmatrix}\nabla\cdot\mathbf{B}\,, \tag{1}$$

which, with the exception of the source term on the right-hand side of the equation, is the divergence form typically in solving systems of conservation laws. The source term is present so that any local deviations from $\nabla\cdot\mathbf{B}$ are handled correctly. In this form, the quantity $(\nabla\cdot\mathbf{B})/\rho$ is treated as a passive scalar; any $(\nabla\cdot\mathbf{B})/\rho$ that is created is passively convected. This form of

the equations is the symmetrizable form, and has the advantage of Gallilean invariance and the ability to derive an entropy conservation law by a linear combination of the remaining equations. Details of the governing equations and the solution scheme are given in the attached paper, which has been submitted to *Journal of Computational Physics.*

Equation 1 is solved by a Roe scheme (Reference 1), an HLLE scheme (Reference 4) or a Boltzmann scheme (Reference 5) derived from the eigensystem of the quasilinear form of Equation 1. Time-stepping is done explicitly, and the entire algorithm has been tied into a solution-adaptive code. Representative results are shown in Figures 10–13. Figure 10 shows the grid used in the set of calculations; the geometry is a simple arc tunnel. The grid is adaptively refined automatically so as to resolve the anode, cathode, and the arc. Figures 11–13 show the current density, acoustic Mach number and plasma density in the arc tunnel for the three solvers. The Boltzmann scheme is the most diffusive, but also the least expensive computationally. The HLLL scheme is is substantially less diffusive, only slightly more expensive, and quite robust. The Roe scheme is the least diffusive, costs about 50% more than the Boltzmann scheme, but is not as robust as the HLLL scheme. Figures 14 and 15 show detailed results for the Roe scheme.

In problems in which the magnetic field is particularly strong, the total energy can be dominated by the $\mathbf{B} \cdot \mathbf{B}$ term. Often in these cases, however, the strong magnetic field is very close to a known solution, for example, a dipole field. Writing the governing in terms of the perturbation from a known field $\mathbf{B}_0$ eliminates the $\mathbf{B}_0 \cdot \mathbf{B}_0$ terms in the equations, thereby eliminating some numerical difficulties. It is not unusual for $\mathbf{B}_0$ to be several orders of magnitude larger than the perturbation field; this subtraction technique substantially increases the accuracy with which the perturbation field is resolved. It is important, however, to do this subtraction intelligently. The resulting Riemann solver, in which the unknowns are based on the perturbation magnetic field, has been developed, tested, and written up for submission to a journal (Reference 1). The treatment that allows this approach to be parallelized, achieving linear speed-ups even on hundreds of processors, was reported at the Supercomputing conference (Reference 2).

The basic geometry generation capabilities of the code developed by Charlton (Reference 3) have been extended to allow parametric definition of arc-constrictor geometries. This tool allows generation of these geometries with almost any combination of dimensions in a matter of minutes. Initial

grids are generated in a matter of hours using automated, adaptive Cartesian methods, and solution-based adaption allows the code to increase resolution around flow regions of interest such as the arc during flow solution. This allows application of the code to a large range of problems involving MHD and complex geometries; arcjets, magnetoplasmadynamic(MPD) thrusters, and fusion propulsion systems are just a few examples.

References

1. K.G. Powell, D.L. De Zeeuw, T.I. Gombosi, T. Linde and P.L. Roe, A Parallel, Solution-Adaptive Upwind Scheme for Magnetohydrodynamics, submitted to *Journal of Computational Physics*, 1998.

2. Q. Stout and D. De Zeeuw and T. Gombosi and C. Groth and H. Marshall and K. Powell, "Adaptive blocks: A high-performance data structure," *Supercomputing*, 1997.

3. E. F. Charlton and K. G. Powell, "An Octree Solution to Conservation Laws over Arbitrary Regions (OSCAR)," AIAA Paper 97-0198, 1997.

4. T. J. Linde, "A Three-Dimensional Adaptive Multifluid MHD Model of the Heliosphere," PhD Thesis, University of Michigan, 1998.

Doctoral Theses Resulting from Grant

1. T. J. Linde, "A Three-Dimensional Adaptive Multifluid MHD Model of the Heliosphere," PhD Thesis, University of Michigan, 1998.

2. R. S. Myong, "Theoretical and Computational Investigations of Nonlinear Waves in Magnetohydrodynamics," PhD Thesis, University of Michigan, 1997.

3. E. G. Charlton, "An Octree Solution to Conservation Laws over Arbitrary Regions with Applications to Aircraft Aerodynamics," PhD Thesis, University of Michigan, 1997.

Refereed Journal Publications Resulting from Grant

1. Gallimore A. D., Kim, S. W., King, L. B., Foster, J. E., and Gulczinski III, F. S., "Near and Far-Field Plume Studies of a 1 kW Arcjet," *Journal of Propulsion and Power (AIAA)*, Vol. 12, No. 1, Jan.–Feb., 1996, 105-111.

2. T. I. Gombosi, D. L. De Zeeuw, R. M. Haberli and K. G. Powell, "Three-dimensional Multiscale MHD Model of Cometary Plasma Environments," *Journal of Geophysical Research*, vol. 101, No. A7, pp. 15,233–15,253, 1996.

3. G. Agresar, J. Linderman, G. Tryggvason and K. Powell, "An Adaptive Front-Tracking Method for the Motion, Deformation and Adhesion of Circulating Cells," *Journal of Computational Physics*, vol. 143, pp. 346–380, 1998.

4. R. S. Myong and P. L. Roe, "Shock Waves and Rarefaction Waves in Magnetohydrodynamics. Part 1: A Model System," *Journal of Plasma Physics*, vol. 58, pp. 485–519, 1997.

5. R. S. Myong and P. L. Roe, "Shock Waves and Rarefaction Waves in Magnetohydrodynamics. Part 2: The MHD System," *Journal of Plasma Physics*, vol. 58, pp. 521–552, 1997.

6. R. S. Myong, "Analytical Results on MHD Intermediate Shocks," *Geophysical Research Letters*, vol. 24, part 22, pp. 2929-2932, 1997.

7. R. S. Myong and P. L. Roe, "On Godunov-Type Schemes for Magnetohydrodynamics. Part 1: A Model System," *Journal of Computational Physics*, to appear, 1998.

8. K.G. Powell, D.L. De Zeeuw, T.I. Gombosi, T. Linde and P.L. Roe, A Parallel, Solution-Adaptive Upwind Scheme for Magnetohydrodynamics, submitted to *Journal of Computational Physics*, 1998.

9. R.M. Häberli, T.I. Gombosi, M.R. Combi, D.L. DeZeeuw, and K.G. Powell, "Modeling of cometary X-rays caused by solar wind minor ions," *Science*, May 1997.

10. M. Combi, K. Kabin, T. Gombosi, D. DeZeeuw and K. Powell, "Io's plasma environment during the Gallileo flyby: Global 3D MHD modeling with adaptive mesh refinement," *JGR Space Physics*, vol. 103, pp. 9071–9081, 1998.

11. R. M. Häberli, M. R. Combi, T. I. Gombosi, D. L. DeZeeuw and K. G. Powell, "Quantitative Analysis of $H_2 0$ Coma Images Using a Multiscale MHD Model with Detailed Ion Chemistry," *Icarus*, vol. 130, pp. 373–386, 1997.

12. T.J. Linde, T.I. Gombosi, P.L.Roe, K.G. Powell, D.L. DeZeeuw, "The heliosphere in the magnetized local interstellar medium: Results of a 3D MHD simulation," *J. Geophys. Res.*, to appear, 1998.

13. P. Song, T.I. Gombosi, T.I., D.L. DeZeeuw, and K.G. Powell, "A model of solar wind –magnetosphere – ionosphere coupling for northward IMF," *Geophys. Res. Lett.*, to appear, 1998.

Selected Other Publications Resulting from Grant

1. Q. Stout and D. De Zeeuw and T. Gombosi and C. Groth and H. Marshall and K. Powell, "Adaptive blocks: A high-performance data structure," *Supercomputing*, 1997.

2. E. F. Charlton and K. G. Powell, "An Octree Solution to Conservation Laws over Arbitrary Regions (OSCAR)," AIAA Paper 97-0198, 1997.

3. K. G. Powell, "Solution of the Euler and Magnetohydrodynamics Equations on Solution-Adaptive Cartesian Grids," *Computational Fluid Dynamics,* Von Kármán Institute for Fluid Dynamics, Lecture Series 1996-06, 1996.

4. Powell, K.G., An approximate Riemann solver for magnetohydrodynamics (that works in more than one dimension), *Upwind and High-Resolution Schemes*, M. Hussaini, B. van Leer and J. van Rosendale, editors, 1997.

Summary Data

- PI Name: Kenneth G. Powell, Bram van Leer and Alec Gallimore
- Grant or Contract Number:F49620-94-1-0399
- Number of Faculty Supported: 3
- Number of Post Doctorates Supported: 0
- Number of Graduate Students: 8
- Others Supported: 0
- Number of Papers in Peer Reviewed Archival Journals: 13
- Number of Peer Reviewed Conference Papers: 2
- Number Of Books: 0
- Number of Book Chapters: 2
- Awards: 1 AIAA Fellow (Van Leer)

Summary

The primary outcomes of this work are:

- An experimental study of the behavior of arc thrusters at various conditions;
- Development of a technique for solving the ideal MHD equations in complex geometries, and its implementation in a solution-adaptive code.

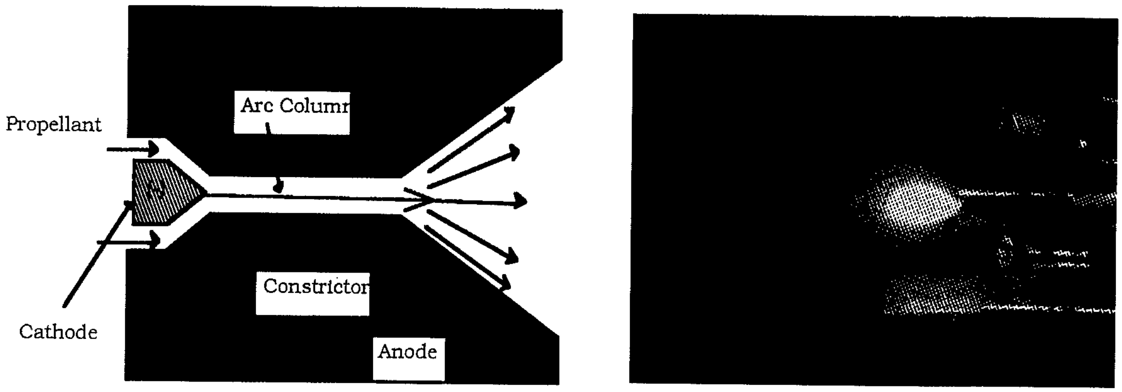

Figure 1: Schematical Diagram and Image of 1-kw-class Arcjet.

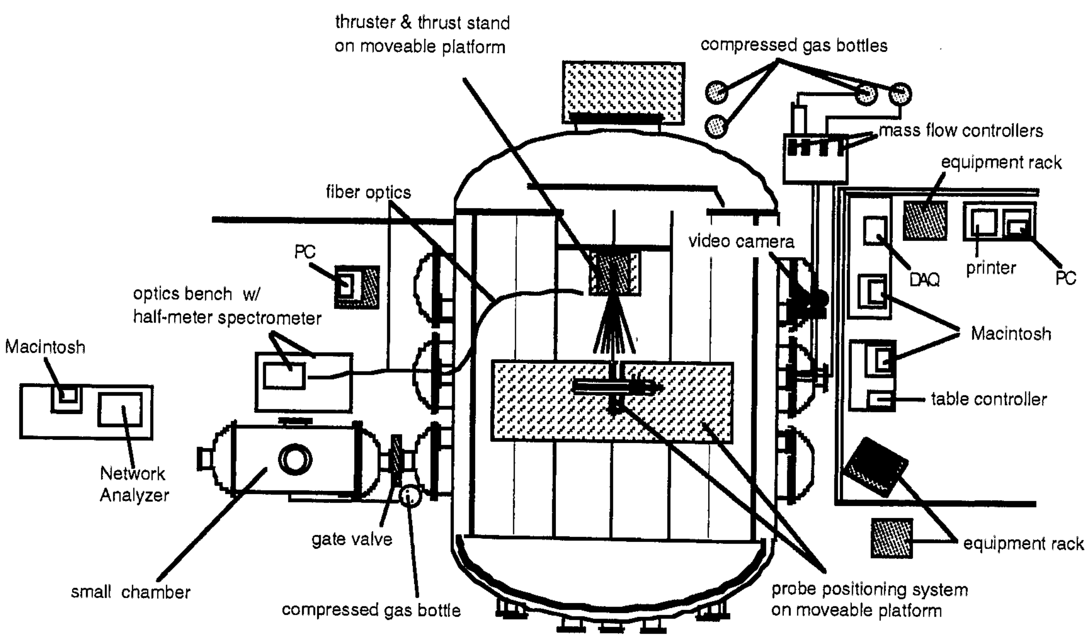

Figure 2: Plasmadynamics and Electric Propulsion Laboratory (PEPL) Facilities.

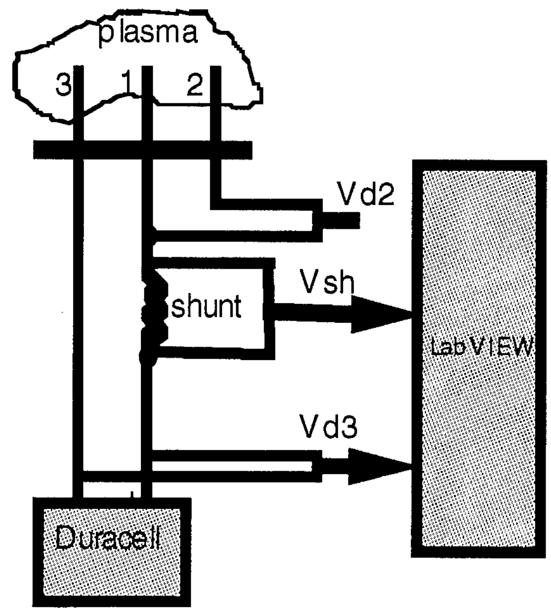

Figure 3: Triple Probe Circuit Used for Near-Field Plume Measruments.

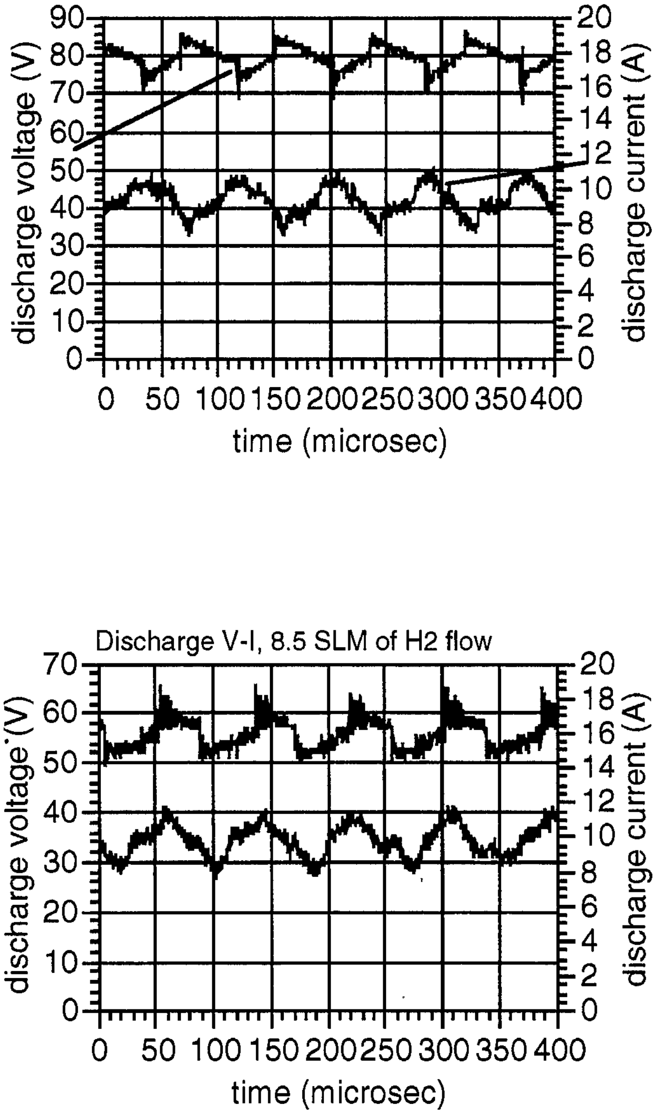

Figure 4: High-Frequency Voltage and Current Oscilloscope Traces.

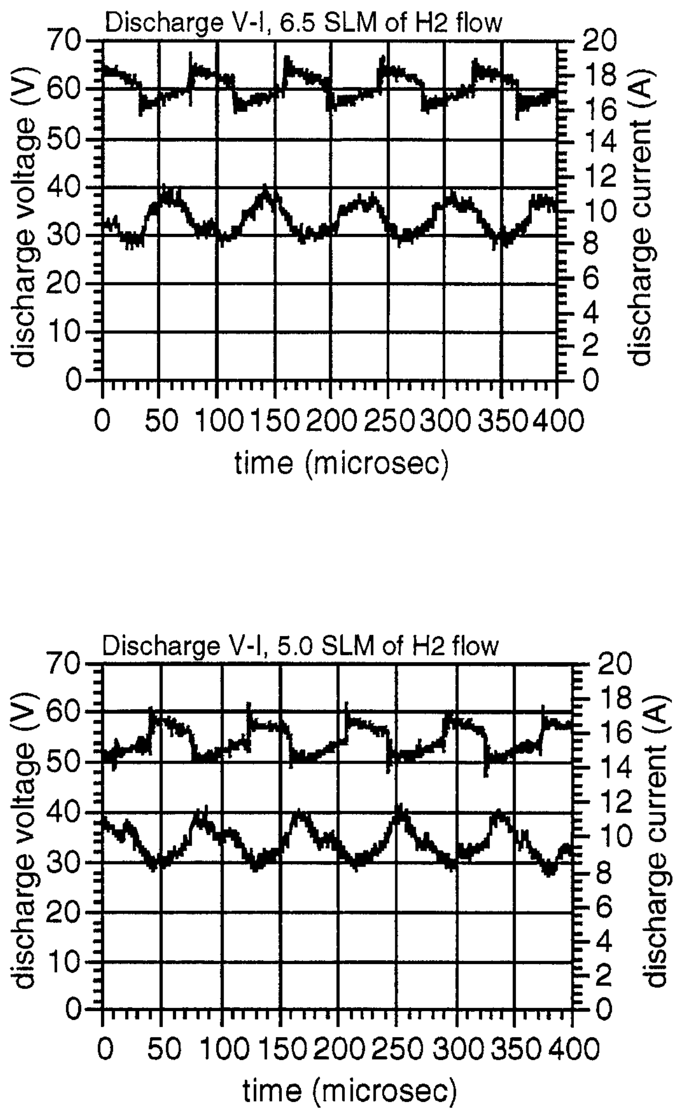

Figure 5: High-Frequency Voltage and Current Oscilloscope Traces.

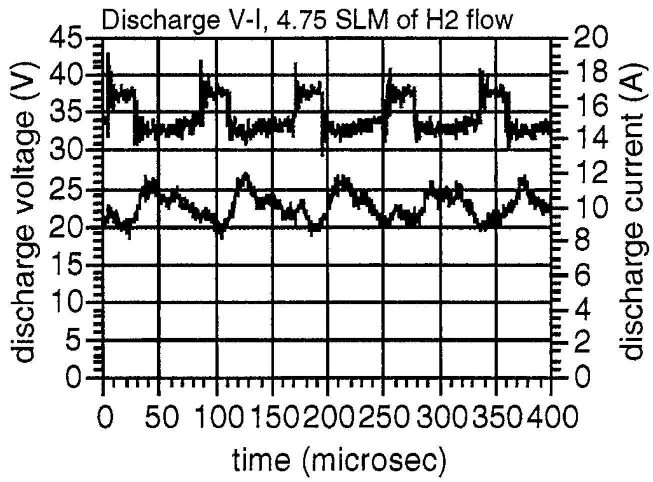

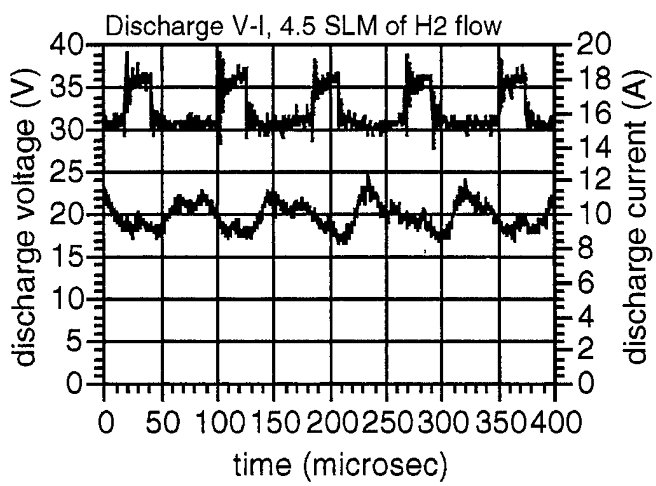

Figure 6: High-Frequency Voltage and Current Oscilloscope Traces.

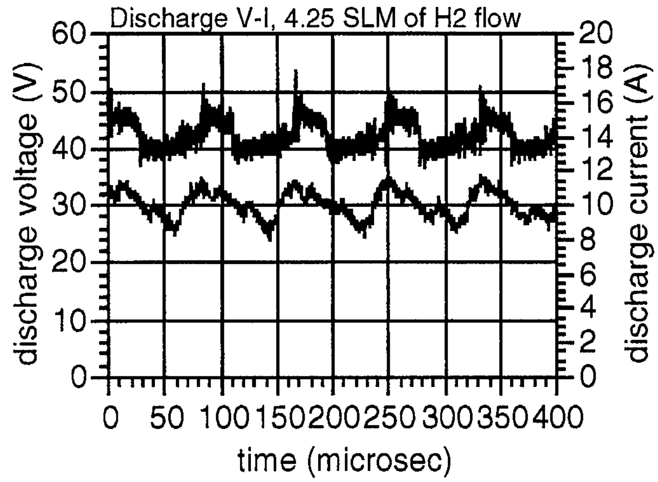

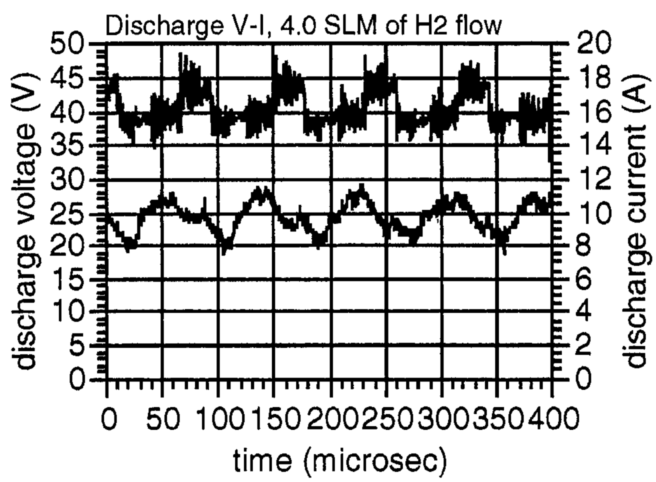

Figure 7: High-Frequency Voltage and Current Oscilloscope Traces.

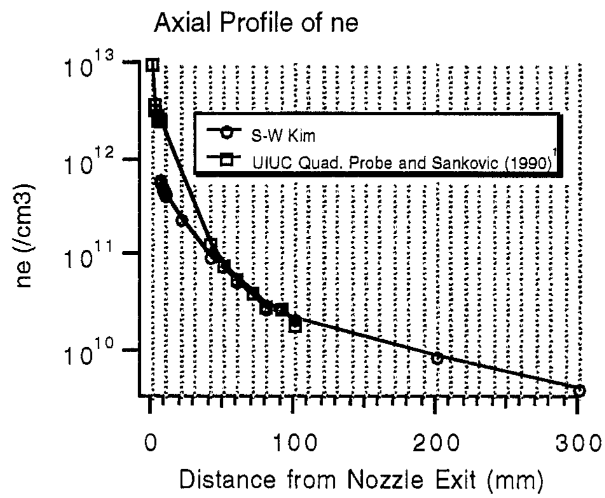

Figure 8: Electron Number Density Axial Profile.

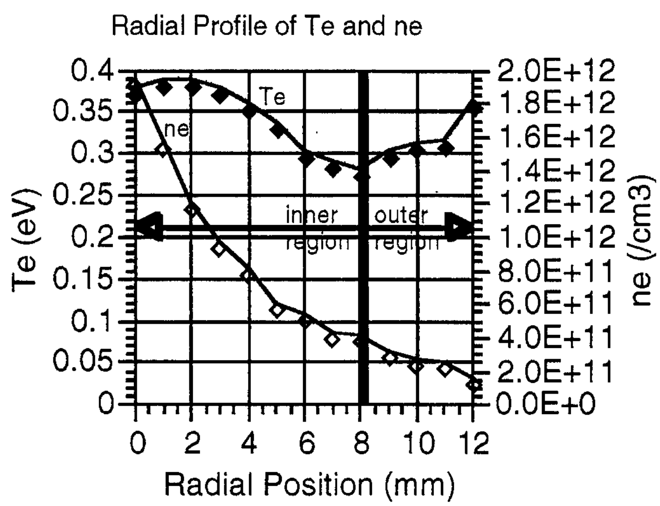

Figure 9: Electron Number Density and Temperature Profile.

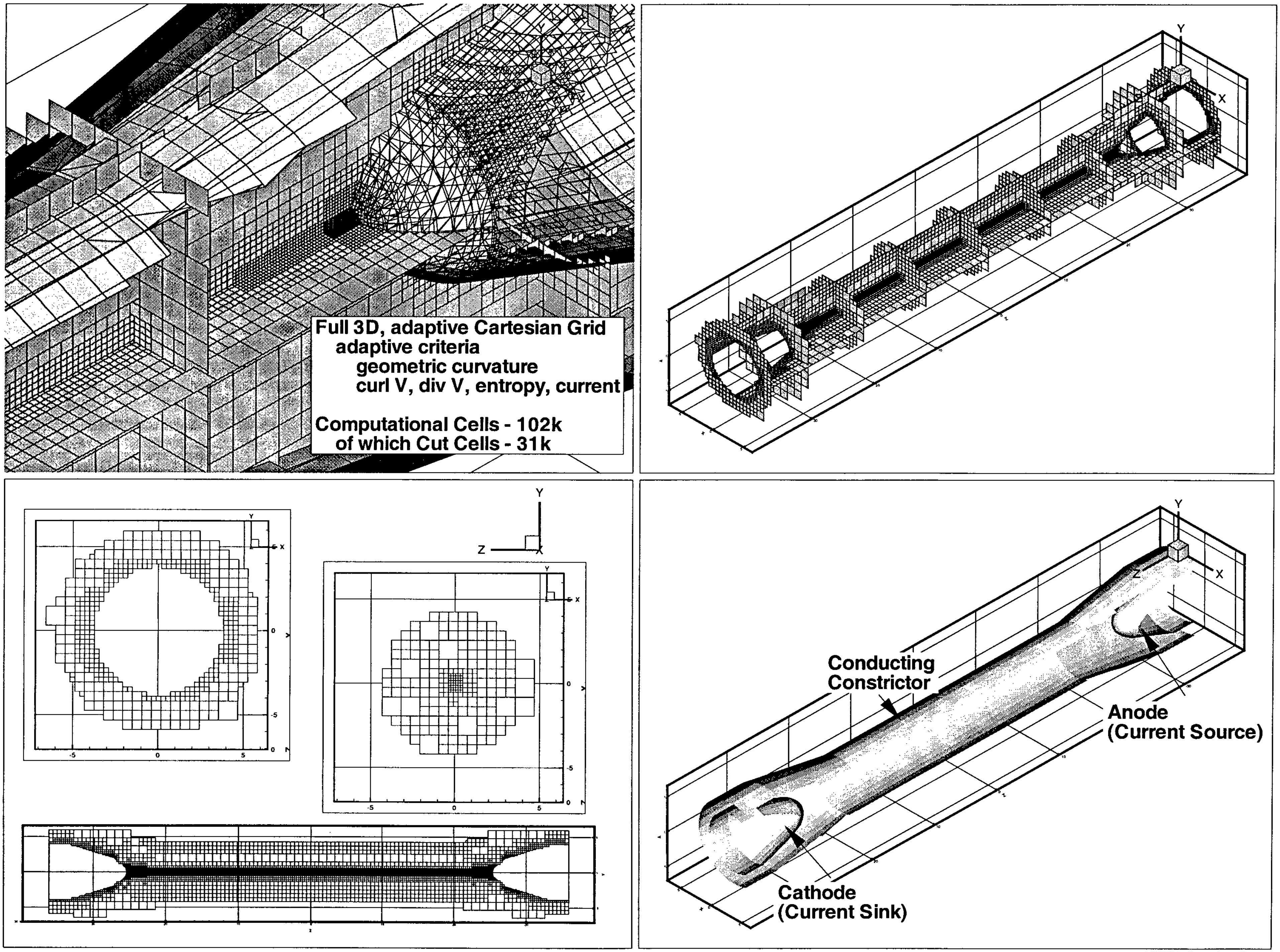
Full 3D, adaptive Cartesian Grid
adaptive criteria
geometric curvature
curl V, div V, entropy, current
Computational Cells - 102k
of which Cut Cells - 31k
Y
X
Z
Conducting
Constrictor
Anode
(Current Source)
Cathode
(Current Sink)

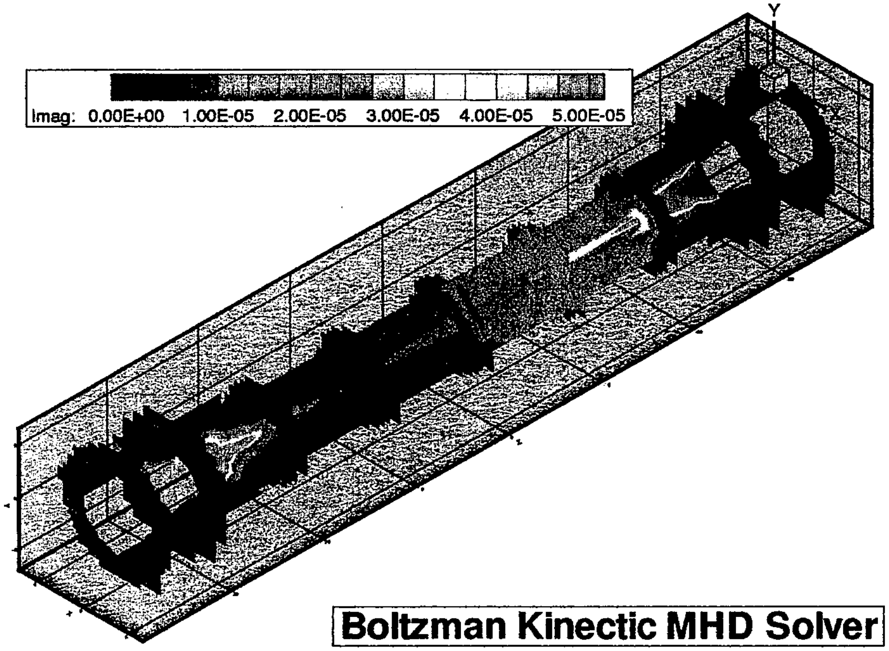

Boltzman Kinectic MHD Solver

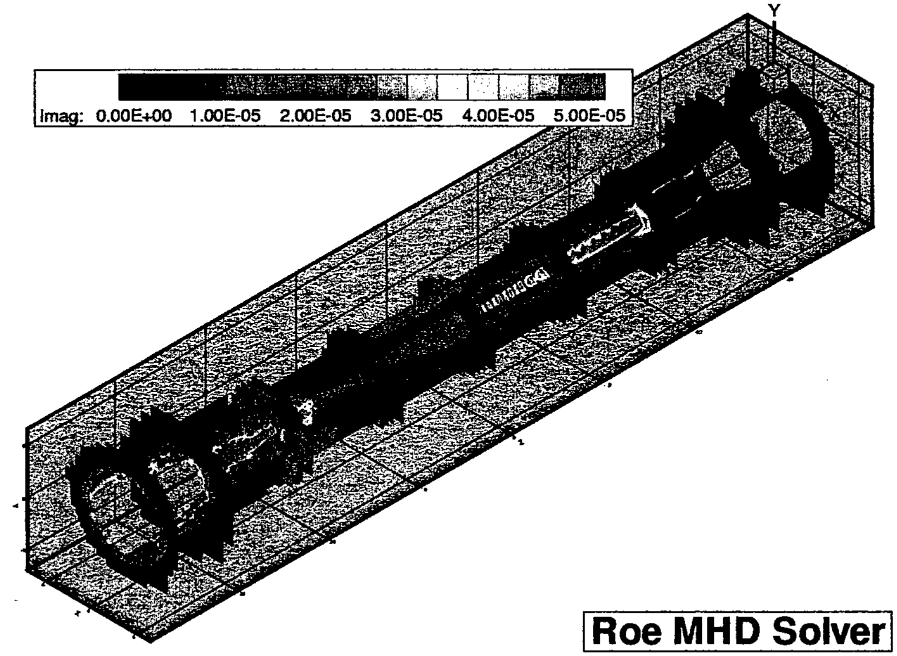

Roe MHD Solver

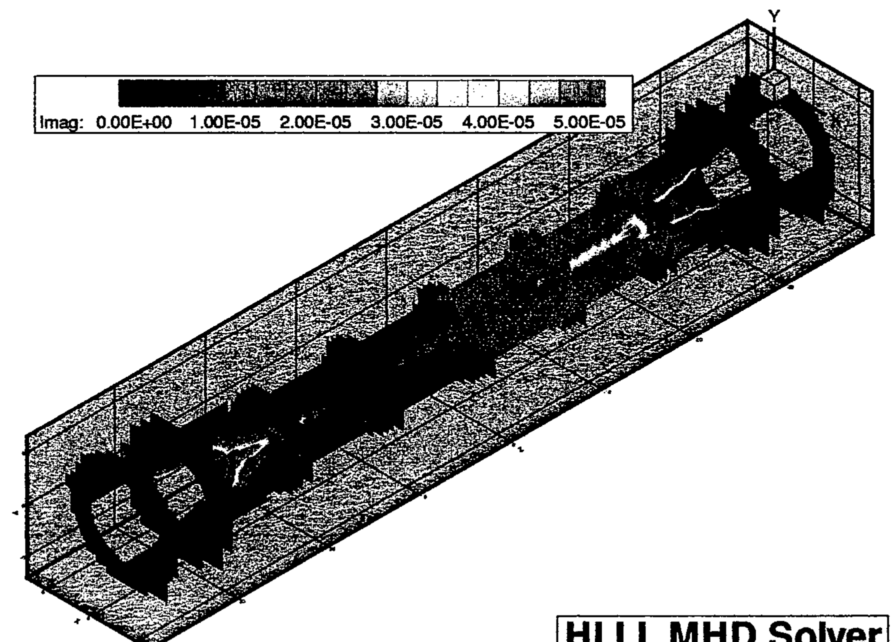

HLLL MHD Solver

I_{mag} = current magnitude

Simulations run 10k iterations with Boltzman solver and then another 1000 iterations with respective solver.

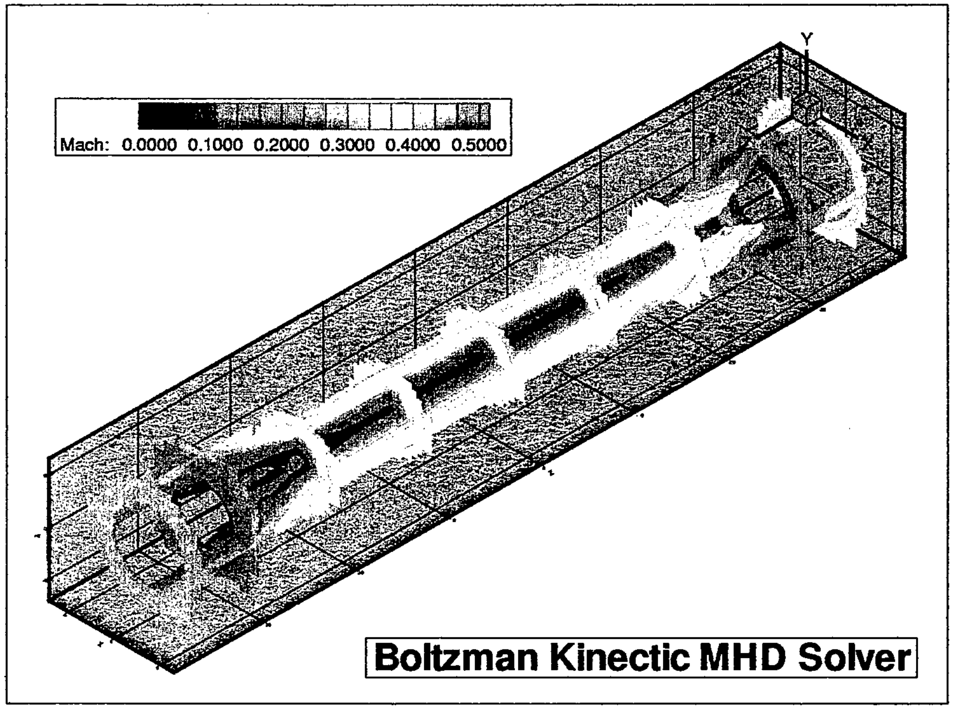

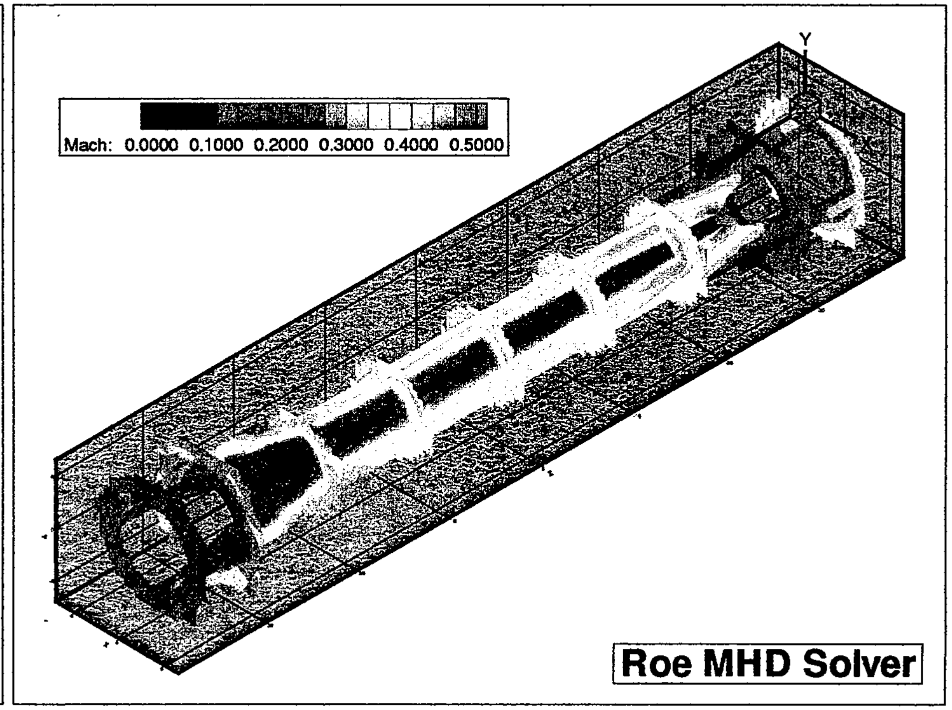

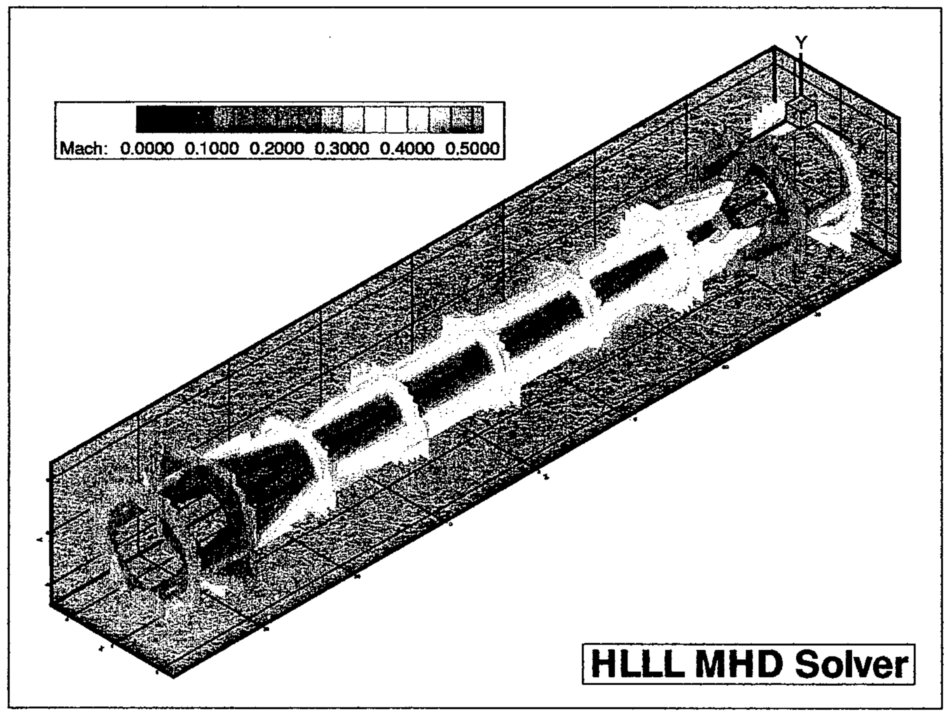

Relative solver speeds

Boltzman Kinectic MHD	1.00
HLLL MHD	1.08
Roe MHD	1.54

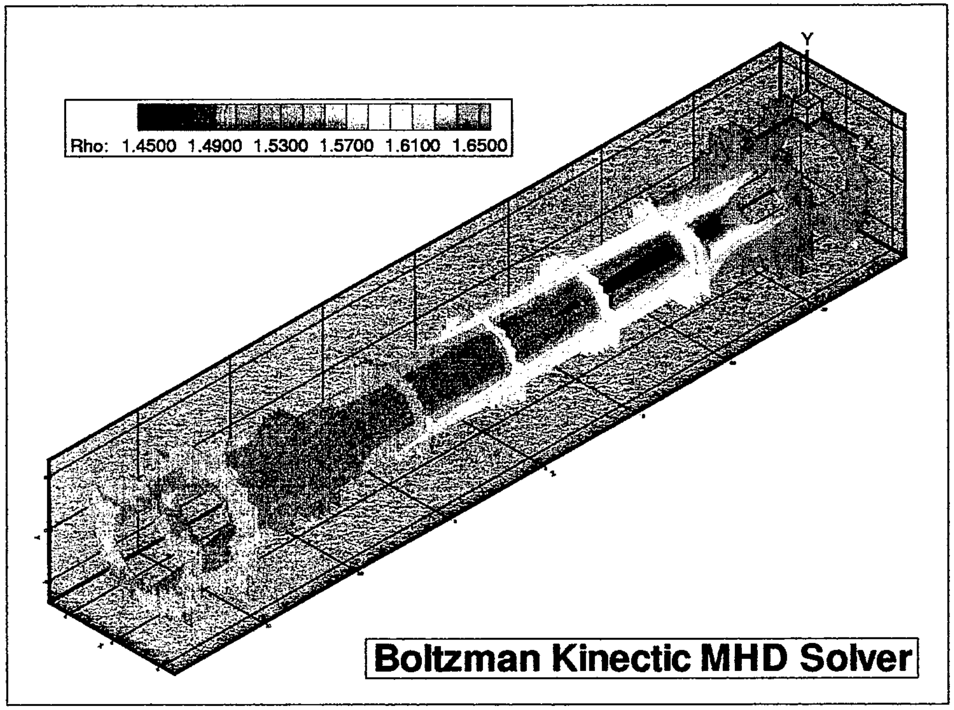
Rho: 1.4500 1.4900 1.5300 1.5700 1.6100 1.6500
Y
X
Boltzman Kinectic MHD Solver

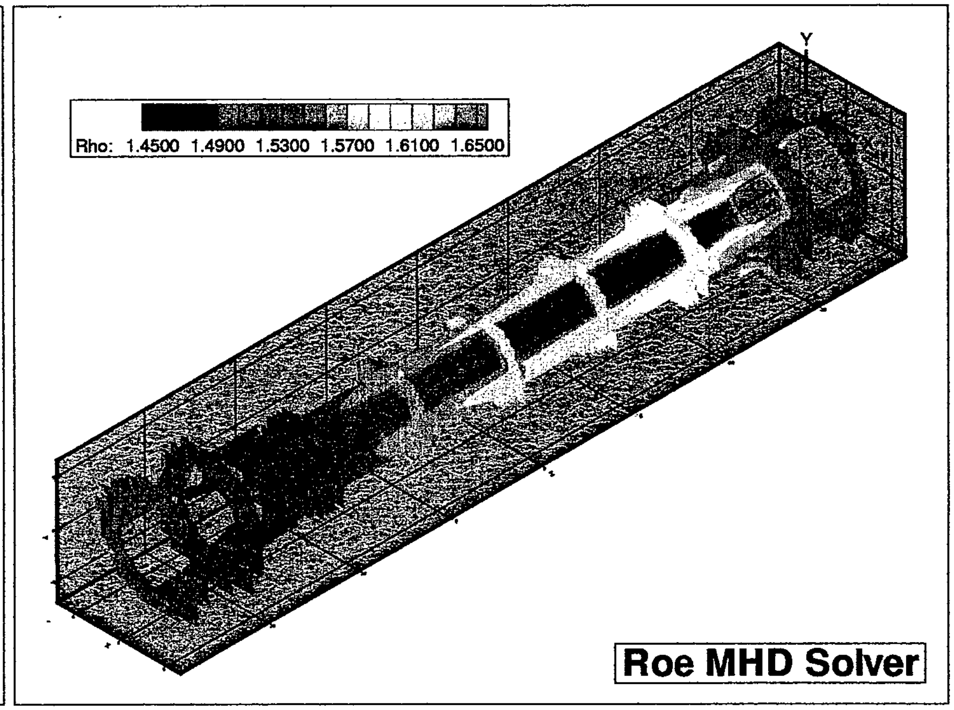
Rho: 1.4500 1.4900 1.5300 1.5700 1.6100 1.6500
Y
Roe MHD Solver

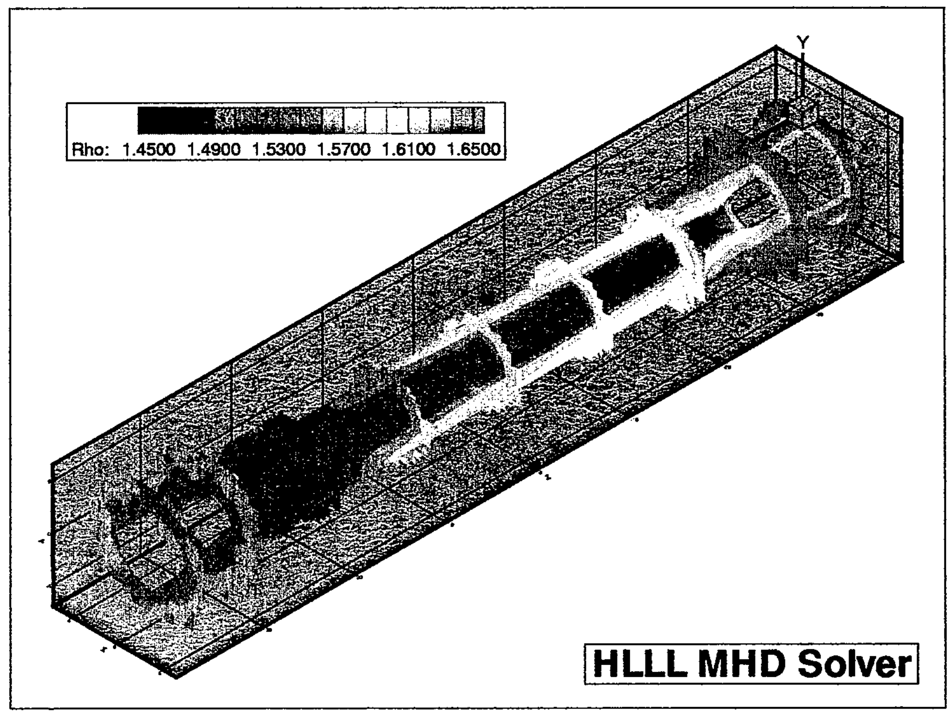
Rho: 1.4500 1.4900 1.5300 1.5700 1.6100 1.6500
Y
HLLL MHD Solver

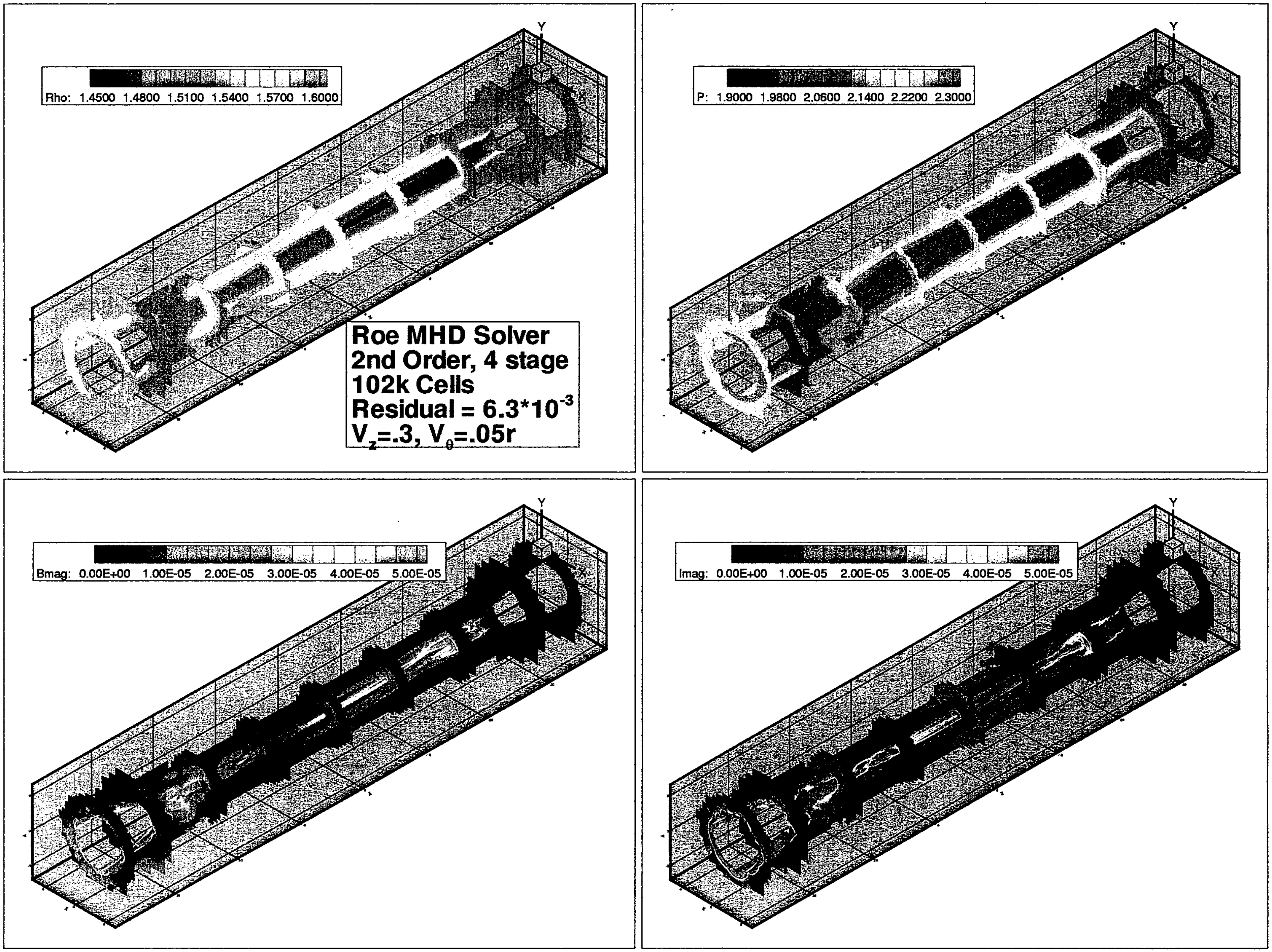
Rho: 1.4500 1.4800 1.5100 1.5400 1.5700 1.6000
Roe MHD Solver
2nd Order, 4 stage
102k Cells
Residual = 6.3*10^-3
V_z=.3, V_θ=.05r
P: 1.9000 1.9800 2.0600 2.1400 2.2200 2.3000
Bmag: 0.00E+00 1.00E-05 2.00E-05 3.00E-05 4.00E-05 5.00E-05
Imag: 0.00E+00 1.00E-05 2.00E-05 3.00E-05 4.00E-05 5.00E-05
Y

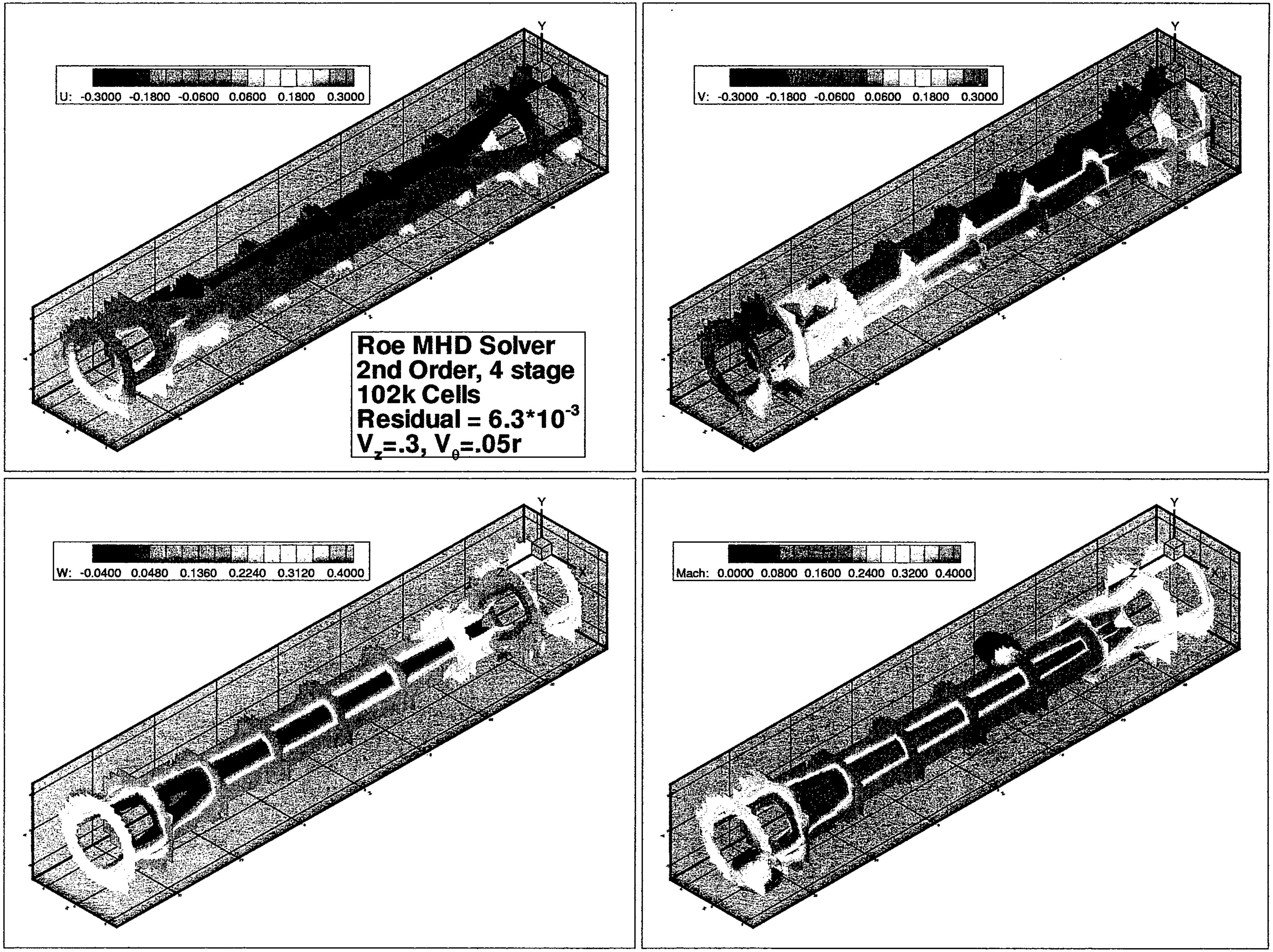
U: -0.3000 -0.1800 -0.0600 0.0600 0.1800 0.3000
V: -0.3000 -0.1800 -0.0600 0.0600 0.1800 0.3000
W: -0.0400 0.0480 0.1360 0.2240 0.3120 0.4000
Mach: 0.0000 0.0800 0.1600 0.2400 0.3200 0.4000
Roe MHD Solver
2nd Order, 4 stage
102k Cells
Residual = 6.3*10^-3
V_z=.3, V_θ=.05r
Y
X
Z